Supporting information

Plasma-catalytic Methanol Synthesis from CO_2 Hydrogenation over Supported Cu cluster Catalyst: Insights in the Reaction Mechanisms

Zhaolun Cui ⊥, Shengyan Meng ⊥, Yanhui Yi *, Amin Jafarzadeh, Shangkun Li, Erik C Neyts, Yanpeng Hao, Licheng Li, Xiaoxing Zhang*, Xinkui Wang, Annemie Bogaerts

Corresponding author: Yanhui Yi, Xiaoxing Zhang

Email: yiyanhui@dlut.edu.cn

Email: xiaoxingzhang@outlook.com

⊥: Z. Cui and S. Meng contributed equally to this paper

1. Experimental details

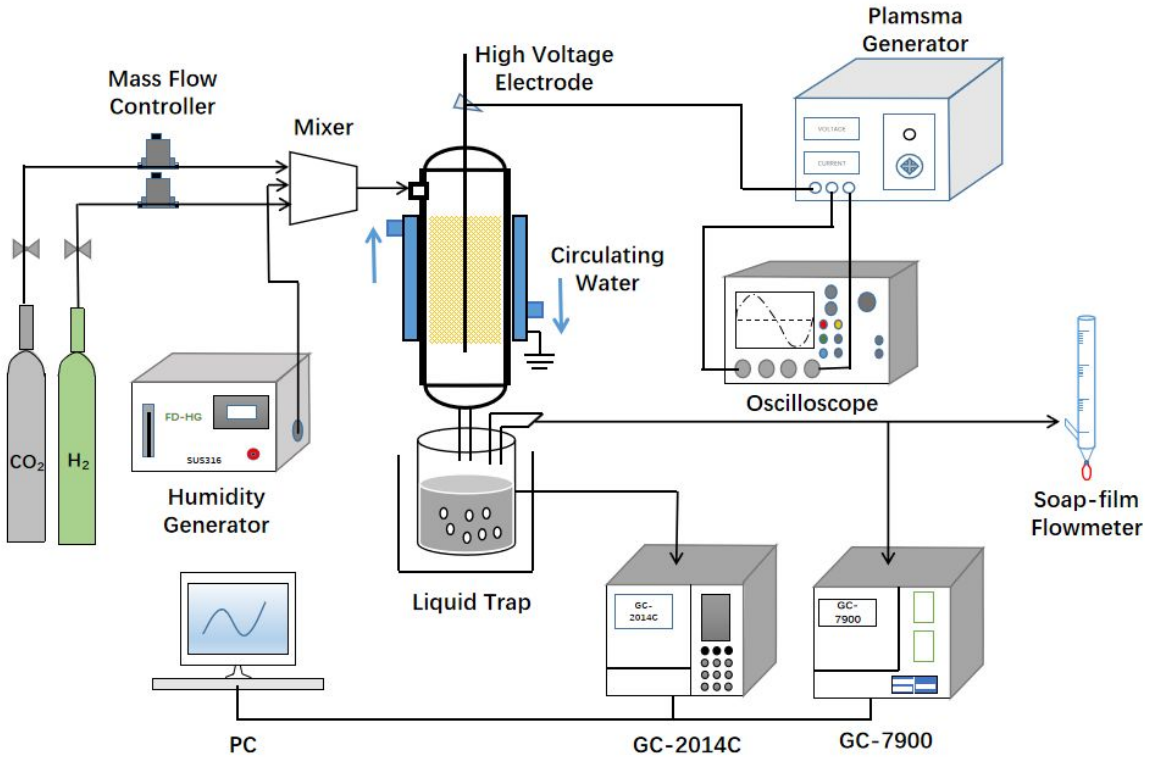

Fig. S1 Diagram of the experimental setup

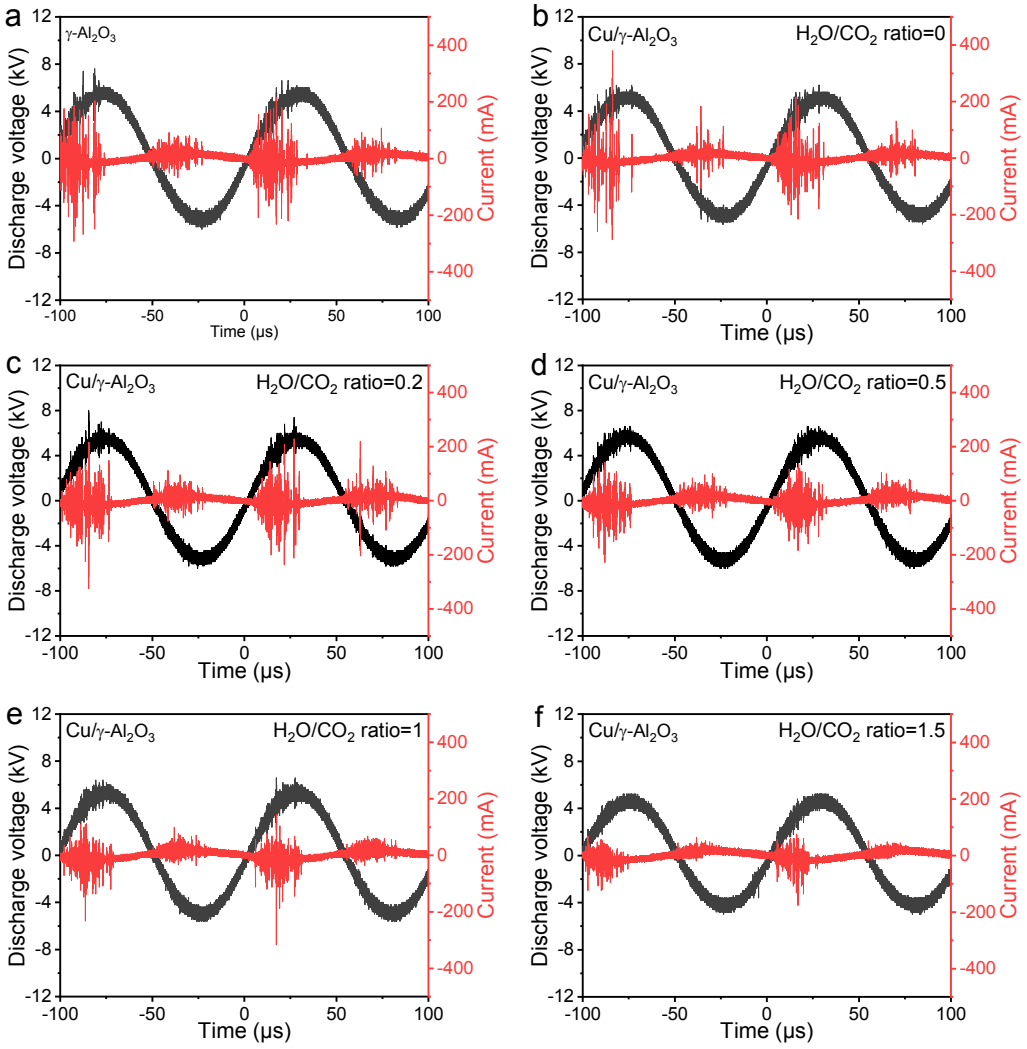

Fig. S2 Waveforms of discharge voltage and current for different plasma-catalytic conditions (CO_2 18 mL/min; H_2 54 mL/min; input power 26 W): (a) γ-Al_2O_3; (b-f) 4% Cu/γ-Al_2O_3 with H_2O/CO_2 molar ratio of (b) 0; (c) 0.2; (d) 0.5; (e) 1; (f) 1.5

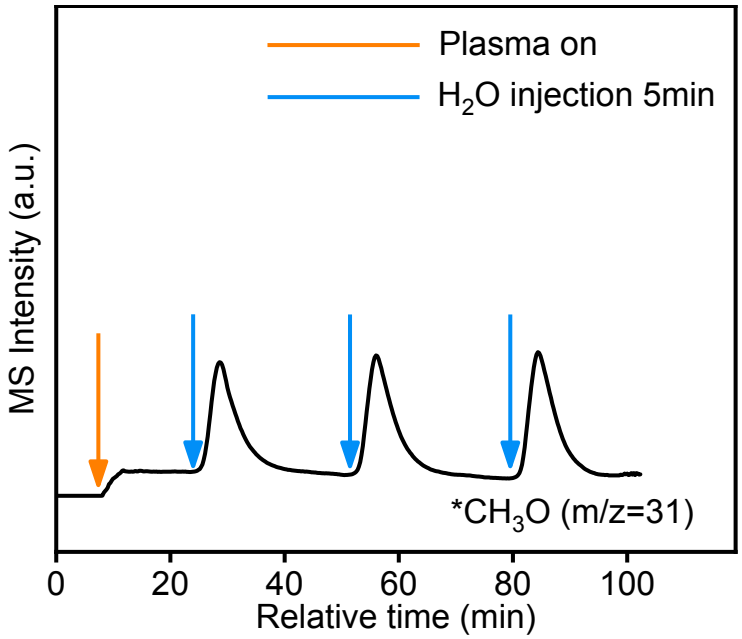

Fig. S3 MS results upon H_2O injection in plasma catalysis

Table S1 Summary of the catalysts, reaction conditions and performance of plasma catalysis and thermal catalysis for CO_2 hydrogenation to methanol. (MR represents the molar ratio of H_2O to CO_2)

Plasma catalysis in this paper

Catalyst	Temperature (°C)	Pressure (MPa)	CO_2 conversion (%)	CH_3OH selectivity (%)	Energy consumption (kJ/mmol)
Cu/Al_2O_3 (0 MR)	60	0.1	9.8	47.5	42.0
Cu/Al_2O_3 (0.1 MR)	60	0.1	8.8	50.2	44.2
Cu/Al_2O_3 (0.2 MR)	60	0.1	8.4	53.0	44.7
Cu/Al_2O_3 (0.5 MR)	60	0.1	6.5	58.7	52.2
Cu/Al_2O_3 (1 MR)	60	0.1	4.2	65.2	75.0

Thermal catalysis

Catalyst	Temperature (°C)	Pressure (MPa)	CO_2 conversion (%)	CH_3OH selectivity (%)	STY (g_{MeOH} kg_{cat}^{-1} h^{-1})
Cu/Al_2O_3 [1]	200	36	8.4	37.3	103
$Cu/ZnO/Al_2O_3$ [2]	260	36	22.7	77.3	7729
$CuO/ZnO/Al_2O_3$ [3]	280	5	19.5	37.0	311
$Cu/Zn/ZrO_2$ [4]	220	3	12.0	71.1	N/A
Cu/Ga/ZnO [5]	270	2	6.0	88.0	378
$Cu/ZnO/ZrO_2/Ga_2O_3$ [6]	250	8	N/A	70.0	382
$Cu/Zn/Ga/SiO_2$ [7]	270	2	5.6	99.5	349
$Pd/ZnO–Al_2O_3$ [8]	180	3	2.9	79.4	N/A
Pd/Zn/CNTs [9]	250	3	6.3	99.6	1187
Au/ZnO [10]	240	0.5	0.3	82.0	N/A
In_2O_3/ZrO_2 [11]	300	5	5.2	99.8	321
MoS_2 [12]	180	5	12.5	94.3	N/A
Al/Pd/ZnO [13]	250	3	14.2	7.3	628
Cu/SiO_2 [14]	250	3	5.2	79.0	N/A
$NiO–In_2O_3$ [15]	250	3	2.8	53.0	256
Pd/CeO_2 [16]	240	3	4.6	25.9	22.8
Cu/C_3N_4 [17]	150	3.2	N/A	95.5	134
PdZn [18]	250	2	7.5	38.7	N/A
Cu@UiO-66 [19]	260	4.5	13.1	78.8	796
ZrO_2/Cu [20]	220	3	4.5	70.0	524
In_2O_3/m-ZrO_2 [21]	280	3	12.1	84.6	N/A
Au/In_2O_3 [22]	275	5	7.7	78.0	470
Pd/ZnO [23]	250	4.5	2.0	80.0	14700
Pd/In_2O_3 [24]	295	3	10.5	72.4	530
Pt/In_2O_3 [25]	300	5	17.3	54.0	542

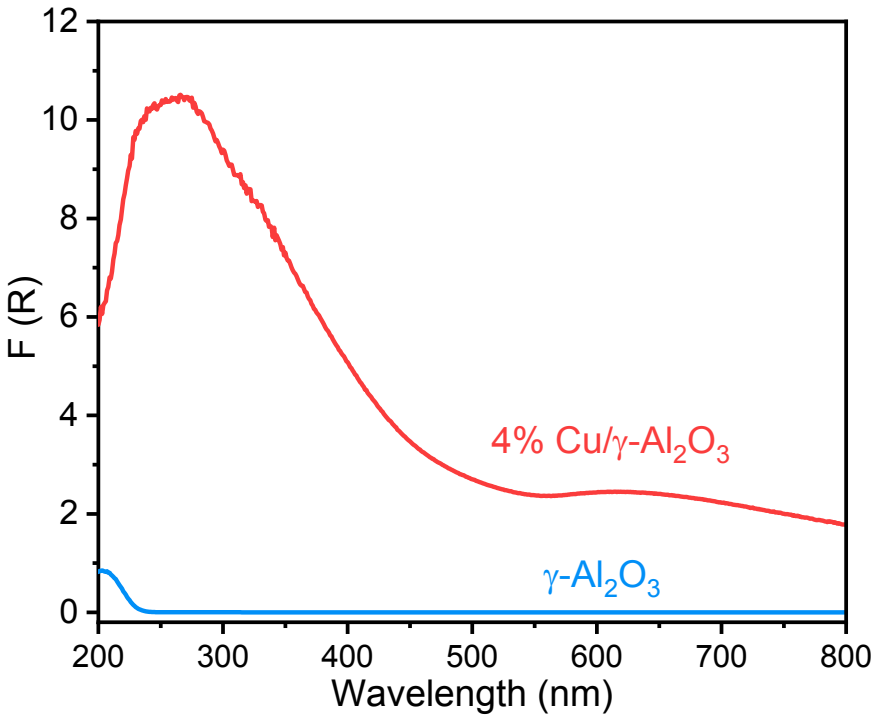

Fig. S4 UV-Vis spectrum of γ-Al_2O_3 and Cu/γ-Al_2O_3.

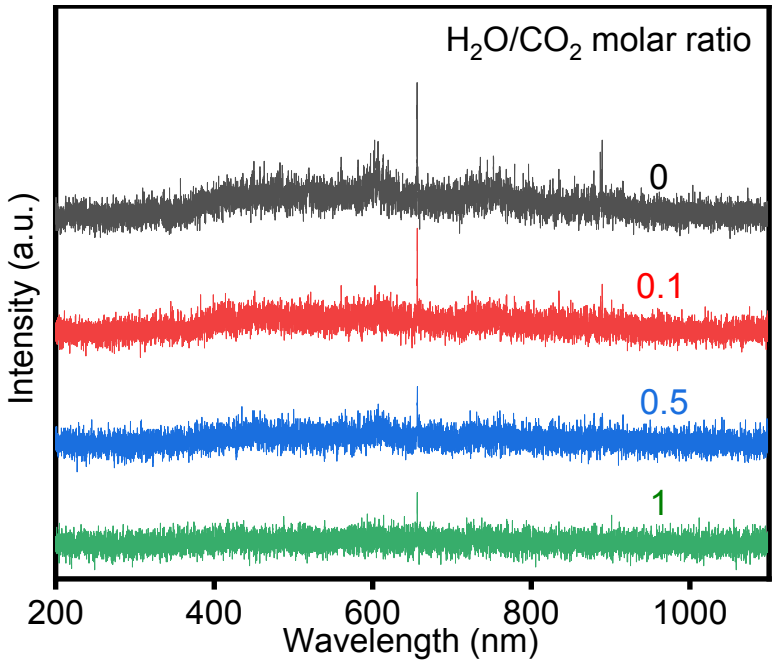

Fig. S5 OES results for different H_2O/CO_2 molar ratios of: 0, 0.1, 0.5 and 1.

Table S2 N_2 physisorption data for different spent catalysts

Spent catalysts (H_2O/CO_2 molar ratio)	S_{BET} ($m^2\ g^{-1}$)	V_{tatol} ($cm^3\ g^{-1}$)	Pore diameter(nm)
γ-Al_2O_3 (0)	134.4	0.45	13.5
Cu/γ-Al_2O_3 (0)	128.0	0.44	12.6
Cu/γ-Al_2O_3 (0.1)	127.7	0.44	12.0
Cu/γ-Al_2O_3 (0.2)	125.4	0.44	12.6
Cu/γ-Al_2O_3 (0.5)	125.1	0.43	12.5
Cu/γ-Al_2O_3 (1)	122.4	0.42	12.2

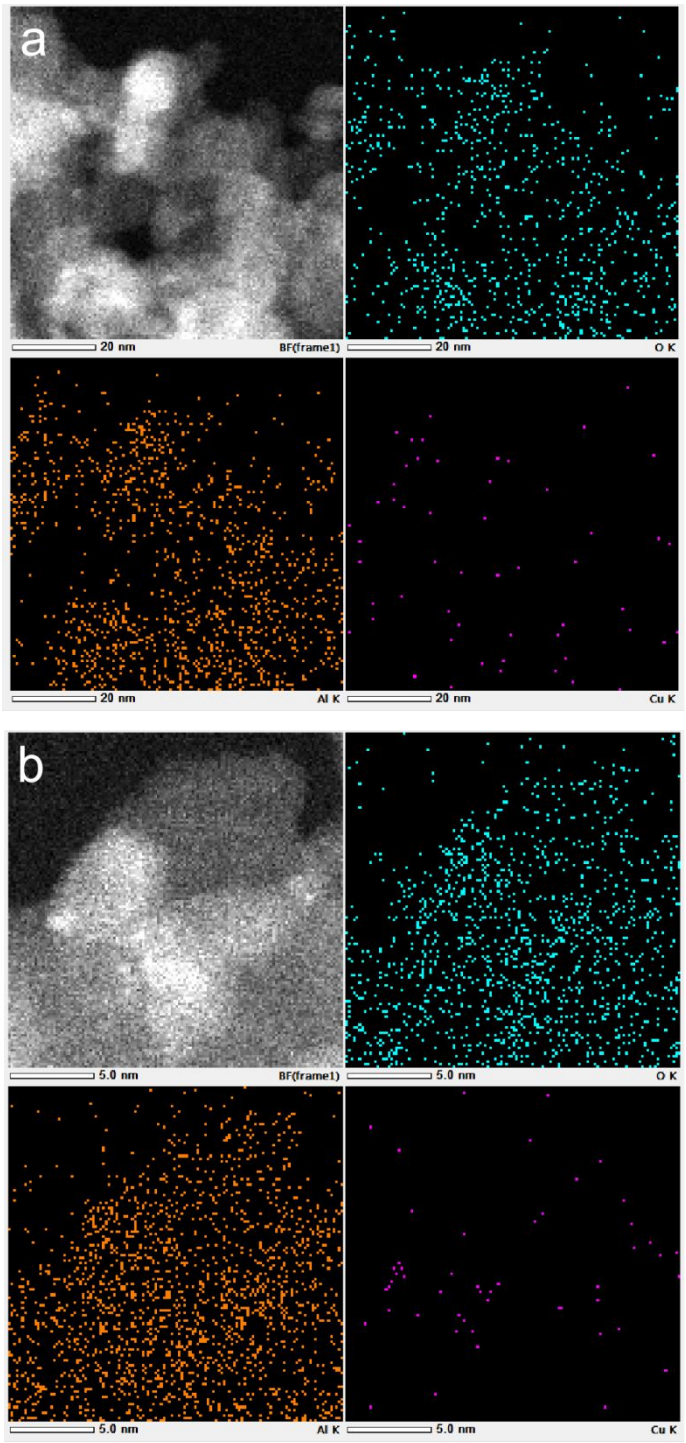

Fig. S6 HAADF-STEM mapping results of Cu/γ-Al_2O_3 catalyst

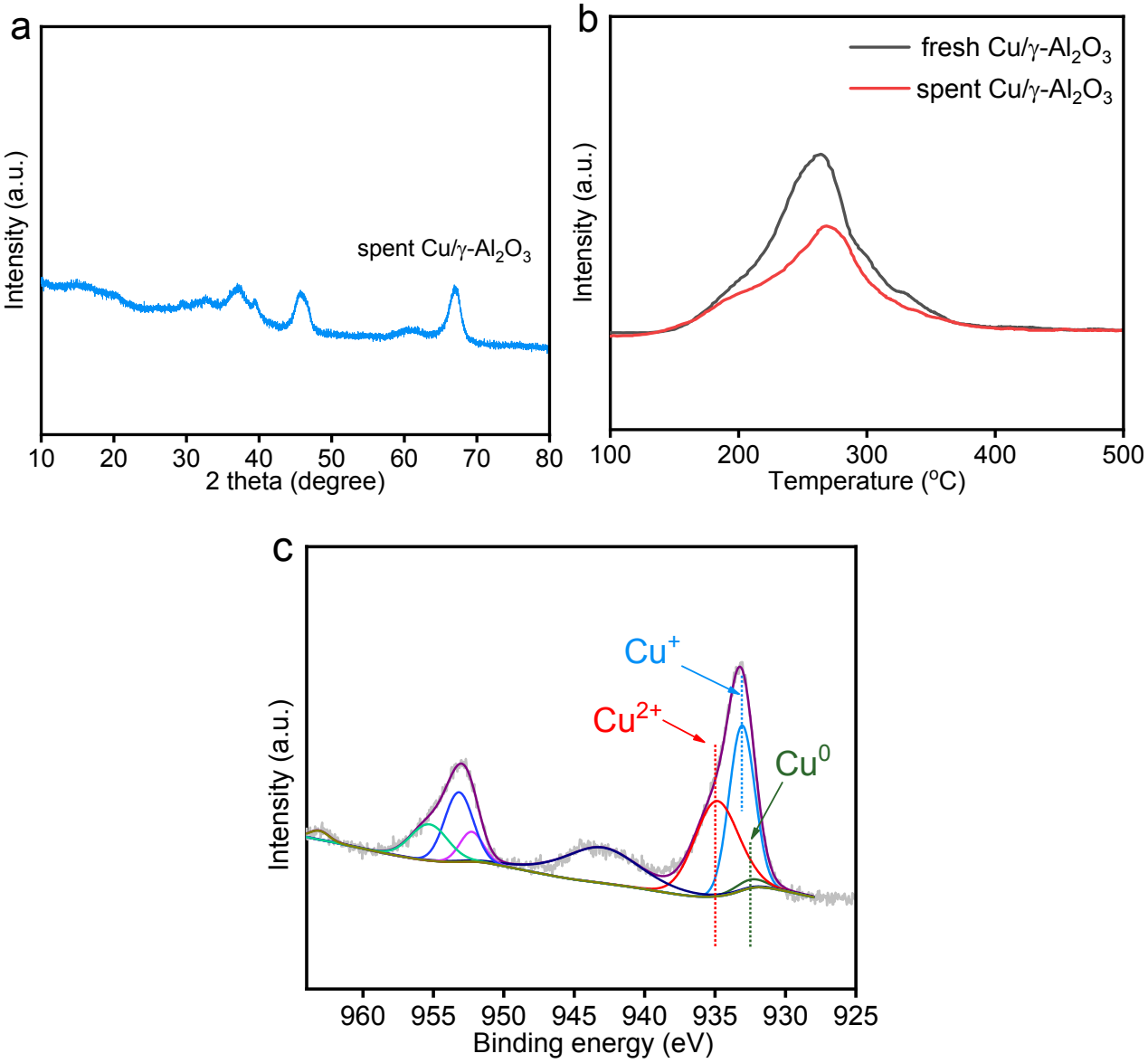

Fig. S7 Characterization of spent Cu/γ-Al_2O_3 catalyst: (a) XRD; (b) TPR; (c) XPS.

2. Choice of the supported cluster model

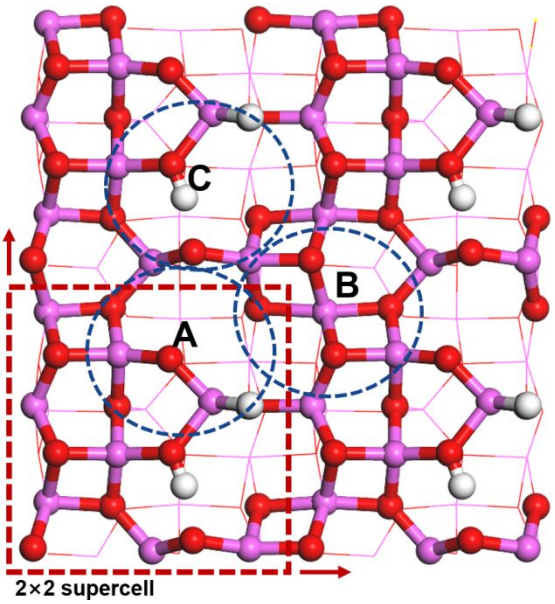

Fig. S8 Typical binding sites for Cu_{13} cluster on the γ-Al_2O_3 (110) surface

The adsorption sites for the hydrated γ-Al_2O_3 (110) surface are chosen according to the study of Marius et al., as shown in Fig. S7.[26] The Cu_{13} cluster is first optimized in the gas phase and then is placed over these three sites. The adsorption test is carried out by static DFT calculations and the most stable configuration at A site is selected to be the main structure for further CO_2 hydrogenation calculations, as shown in Fig. S8. It should be noted that the final configuration is not validated by a molecular dynamic checking, thus the sampling is not complete for the whole system. But this method has been validated to be practical in previous studies and the configuration we use should be able to represent the supported Cu_{13} cluster model to provide acceptable results.[26,27]

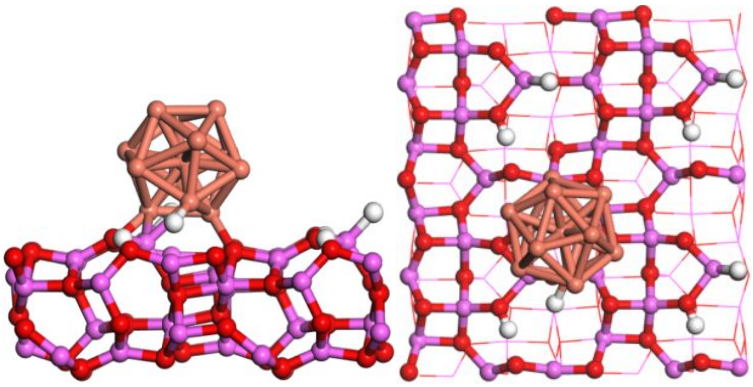

Fig. S9 Stable adsorption configuration of Cu_{13} on the γ-Al_2O_3 (110) surface.

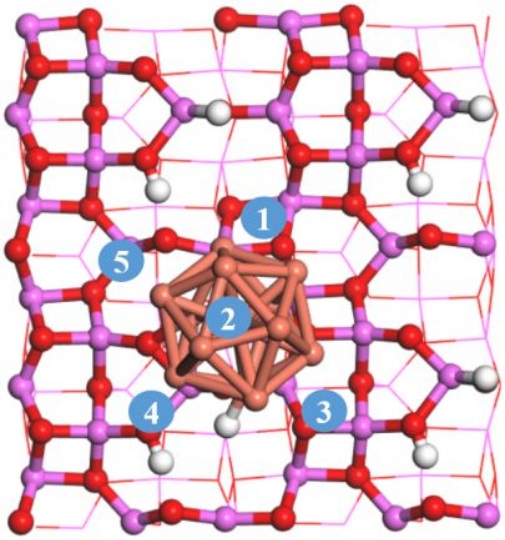

Fig. S10 Five typical adsorption sites on Cu_{13}/γ-Al_2O_3(110): Sites 1, 3, 4 and 5 are four Cu_{13}-Al_2O_3 interface sites. Site 2 is on the top of the Cu_{13} cluster.

3. Computational details

Table S3 Adsorption energy of reactant and product molecules on 5 sites of Cu_{13}/γ-Al_2O_3 surface (Unit: eV)

site	CO_2	H_2	CH_3OH	H_2O
1	-0.72	-0.34	-0.94	-1.12
2	-0.78	-0.37	-0.84	-0.80
3	-1.29	-1.37	-1.45	-1.36
4	-1.14	-0.07	-1.25	-0.68
5	-0.09	-0.07	-0.19	-0.22

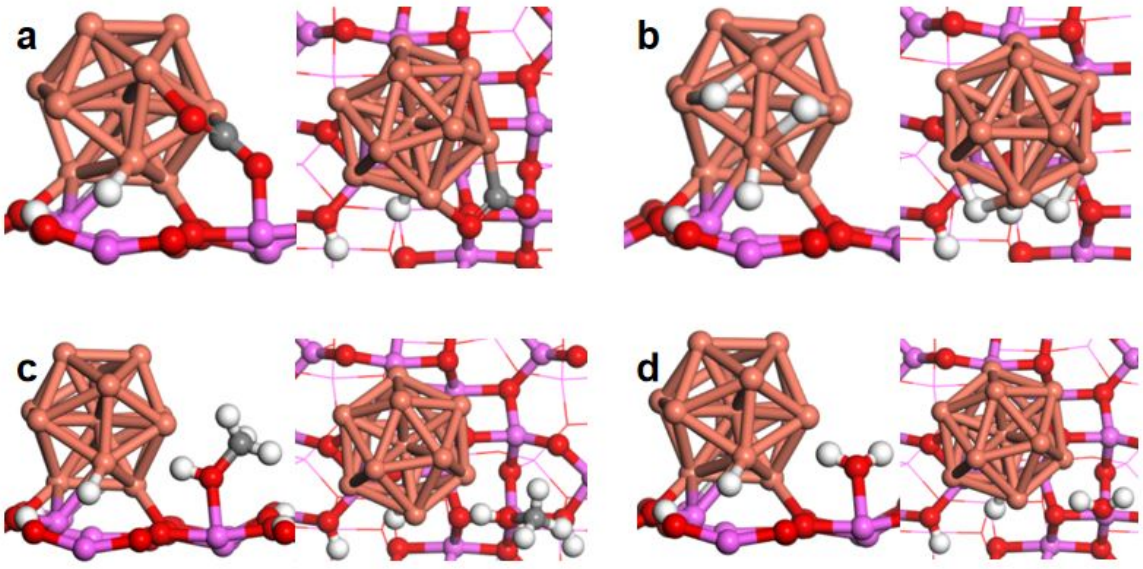

Fig. S11 Most stable configurations of four molecules. H_2 is automatically decomposed into two adsorbed H* atoms without barrier. (a) CO_2; (b) H_2; (c) CH_3OH; (d) H_2O.

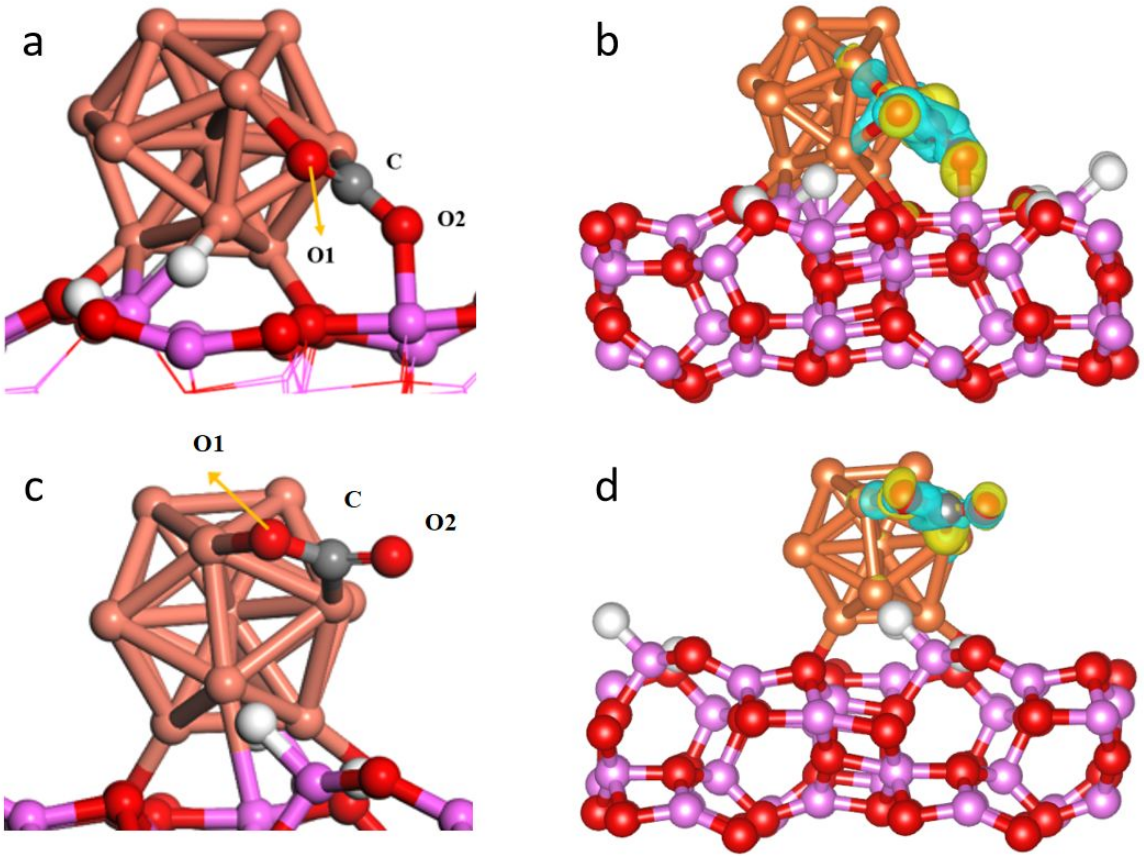

Fig. S12 CO_2 adsorption configuration and electronic properties: (a) Adsorption configuration of CO_2 at Cu_{13}/γ-Al_2O_3 interface; (b) Charge density difference of CO_2 adsorption at Cu_{13}/γ-Al_2O_3 interface: cyan and yellow parts mean charge density increase and decrease, respectively; (c) Adsorption configuration of CO_2 on Cu_{13} cluster; (d) Charge density difference of CO_2 adsorption on Cu_{13} cluster.

Table S4 Binding energy for important intermediates

Adsorbates	Adsorption energy (eV)
CO	-1.98
H_2CO	-2.67
H_2COO	-2.34
HCOOH	-2.01
HCO	-3.10
cis-COOH	-2.89
bi-HCOO	-4.55
H_3CO	-4.52
H_2COH	-2.83
H_2COOH	-3.52
H_2O	-1.35
OH	-4.62

Table S5 Reaction energies and activation barriers

No.	Reaction	Δ*E* (eV)	E_a (eV)
1	$CO_2(g) + * – CO_2*$	-1.28	——
2	$H_2(g) + *+ * – H* + H*$	-0.86	——
3	$CO_2* + H* – bi\text{-}HCOO*$	-0.43	1.23
4	$bi\text{-}HCOO* + H^{a}* – H_2COO*$	0.28	1.16
5	$bi\text{-}HCOO* + H^{b}* – HCOOH*$	0.56	1.32
6	$HCOOH* + H* – H_2COOH*$	0.09	1.03
7	$H_2COOH* – H_2CO* + OH*$	-0.42	0.25
8	$H_2COO* + H*– H_2CO* + OH*$	-0.58	2.11
9	$H_2COO*– H_2CO* + O*$	0.24	1.51
10	$H_2CO* + O* + H* – H_2CO* + OH*$	-0.26	0.01
11	$H_2CO* + OH* +H* – H_2CO* + H_2O*$	-0.29	1.20
12	$CO_2* + H* – trans\text{-}COOH*$	0.29	1.51
13	$trans\text{-}COOH* – cis\text{-}COOH*$	-0.27	——
14	$cis\text{-}COOH* – CO*+ OH*$	-1.14	0.00
15	$CO* + OH* + H* – CO* + H_2O*$	0.88	1.17
16	$CO* + H* – HCO*$	0.19	0.96
17	$HCO* + H* – H_2CO*$	-0.60	0.66
18	$H_2CO* + H^{c}* – H_3CO*$	-0.04	0.79
19	$H_2CO* + H^{d}* – H_2COH*$	-0.43	0.51
20	$H_3CO* + H* – H_3COH*$	-0.36	1.25
21	$H_2COH* + H* – H_3COH*$	0.04	1.27
22	$CH_3OH* – CH_3OH(g) + *$	1.45	——
23	$CO_2* – CO* + O*$	1.06	2.08
24	$H_3CO* – CH_3* + O*$	0.63	2.03
25	$CH_3* + H* – CH_4*$	-0.76	0.66
26	$CH_4* – CH_4(g) + *$	0.24	——
27	$CH_4(g) + O* + H* – CH_4 + OH*$	-0.02	1.87
28	$CH_4(g) + OH* + H* – CH_4 + H_2O*$	1.06	1.64
29	$H(g) + CO_2* – bi\text{-}HCOO*$	——	0.00
30	$H(g) + CO_2* – trans\text{-}COOH*$	——	0.00
31	$H(g) + CO* – HCO*$	——	0.00
32	$H* + CO(g) – HCO*$	——	0.00
33	$H(g) + HCOO* – HCOOH*$	——	0.00
34	$H(g) + H_3CO* – H_3COH*$	——	0.00
35	$H(g) + H_2COH* – H_3COH*$	——	0.00

[a] and [b] correspond to different H* sites for HCOO* hydrogenation

[c] and [d] correspond to different H* sites for H_2CO* hydrogenation

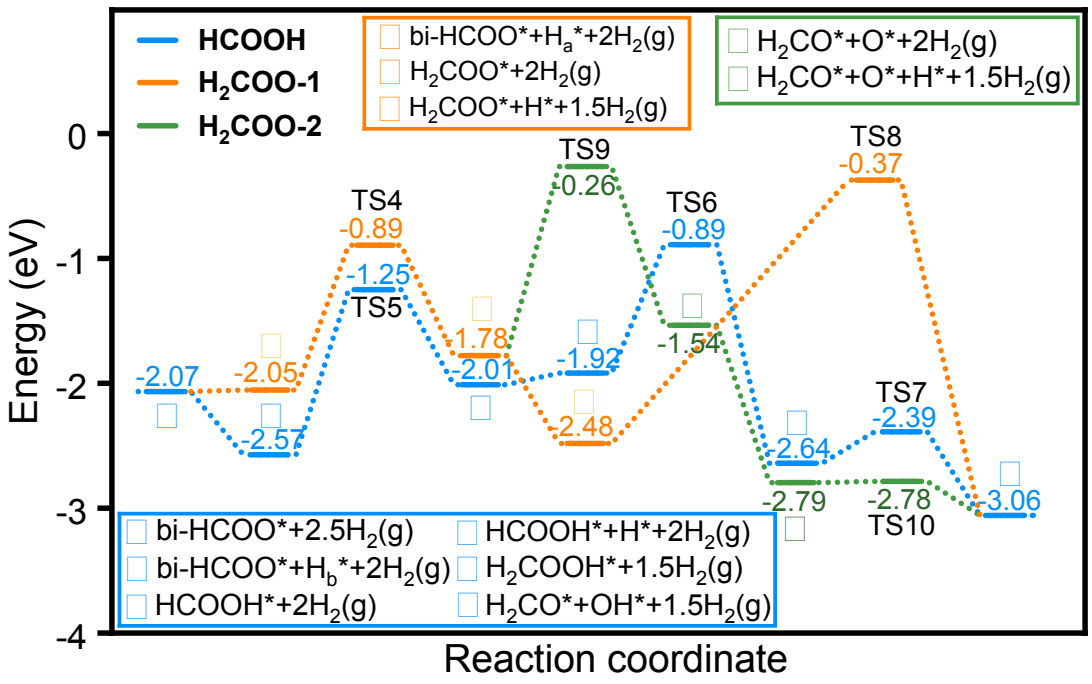

Scheme S1 Three reaction paths from HCOO* to H_2CO* via L-H mechanism

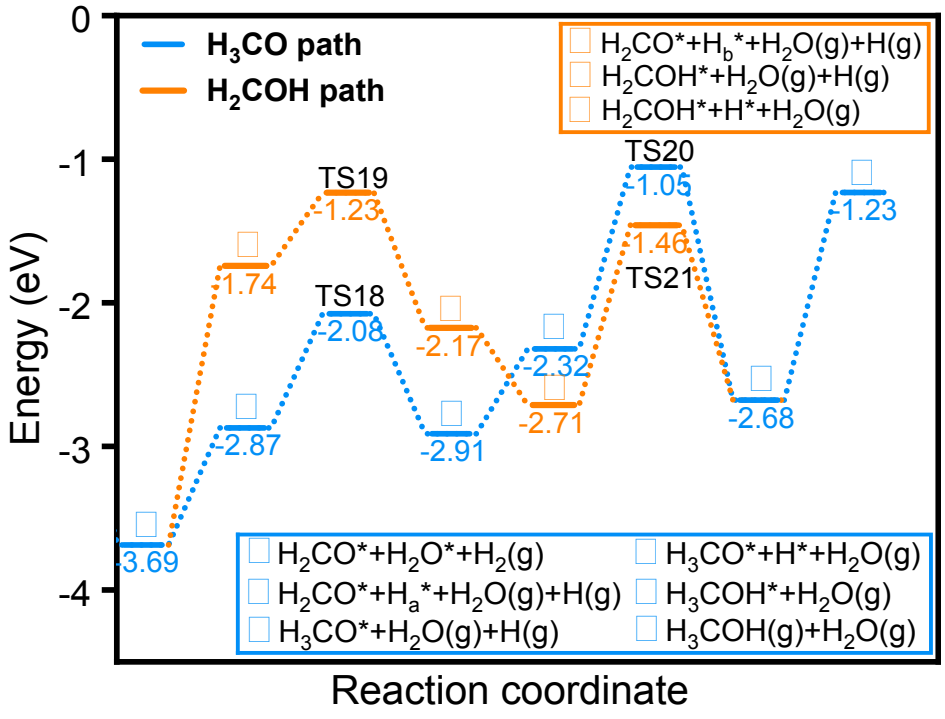

Scheme S2 Energy paths of CH_3OH synthesis from H_3CO* and H_2COH*

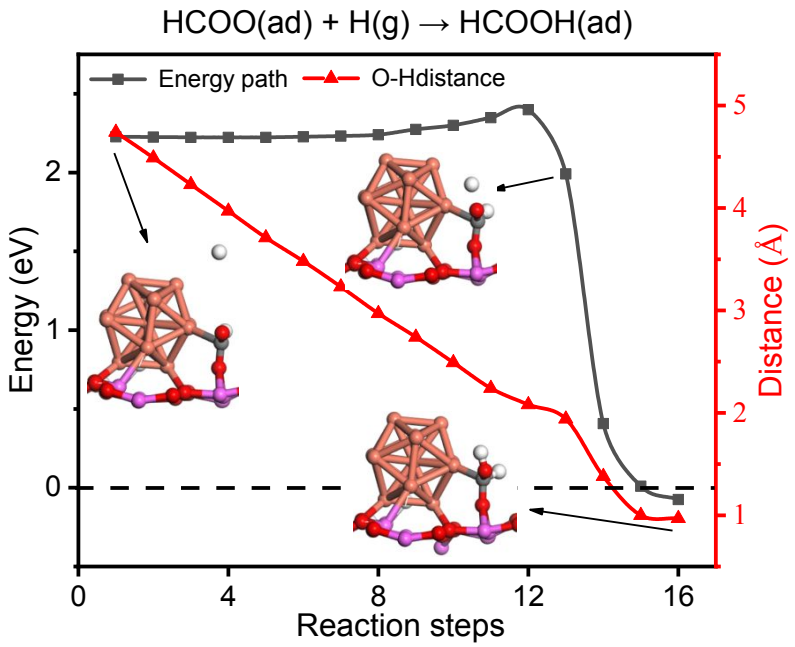

Fig. S13 Formation of HCOOH* via E-R mechanism

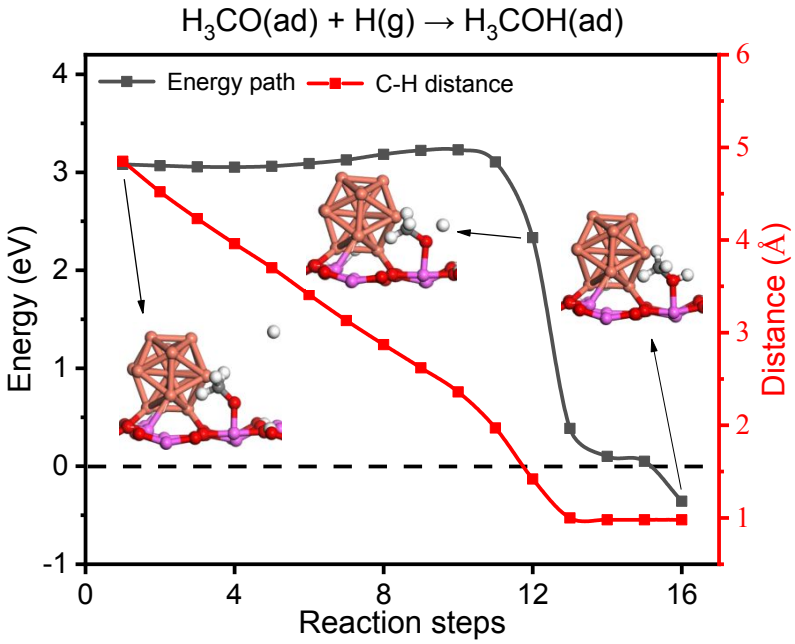

Fig. S14 H_3COH formation via E-R mechanism from H_3CO* and gas phase H(g)

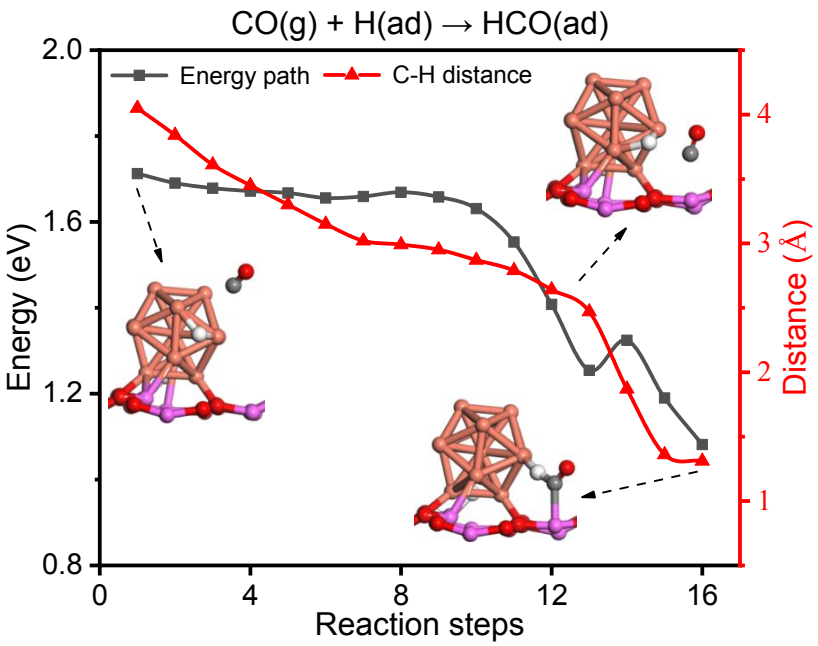

Fig. S15 HCO formation via E-R mechanism from H* and gas phase CO(g)

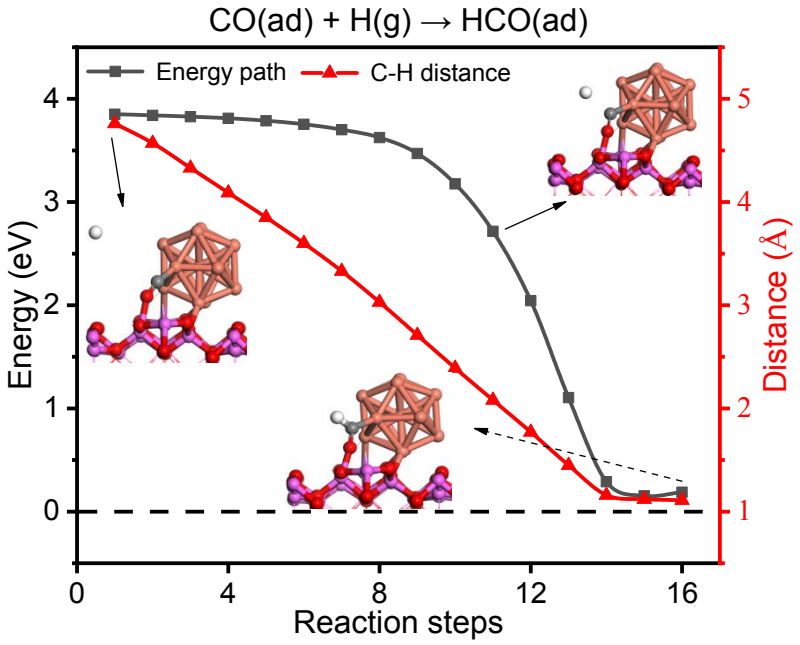

Fig. S16 HCO formation via E-R mechanism from CO* and gas phase H(g)

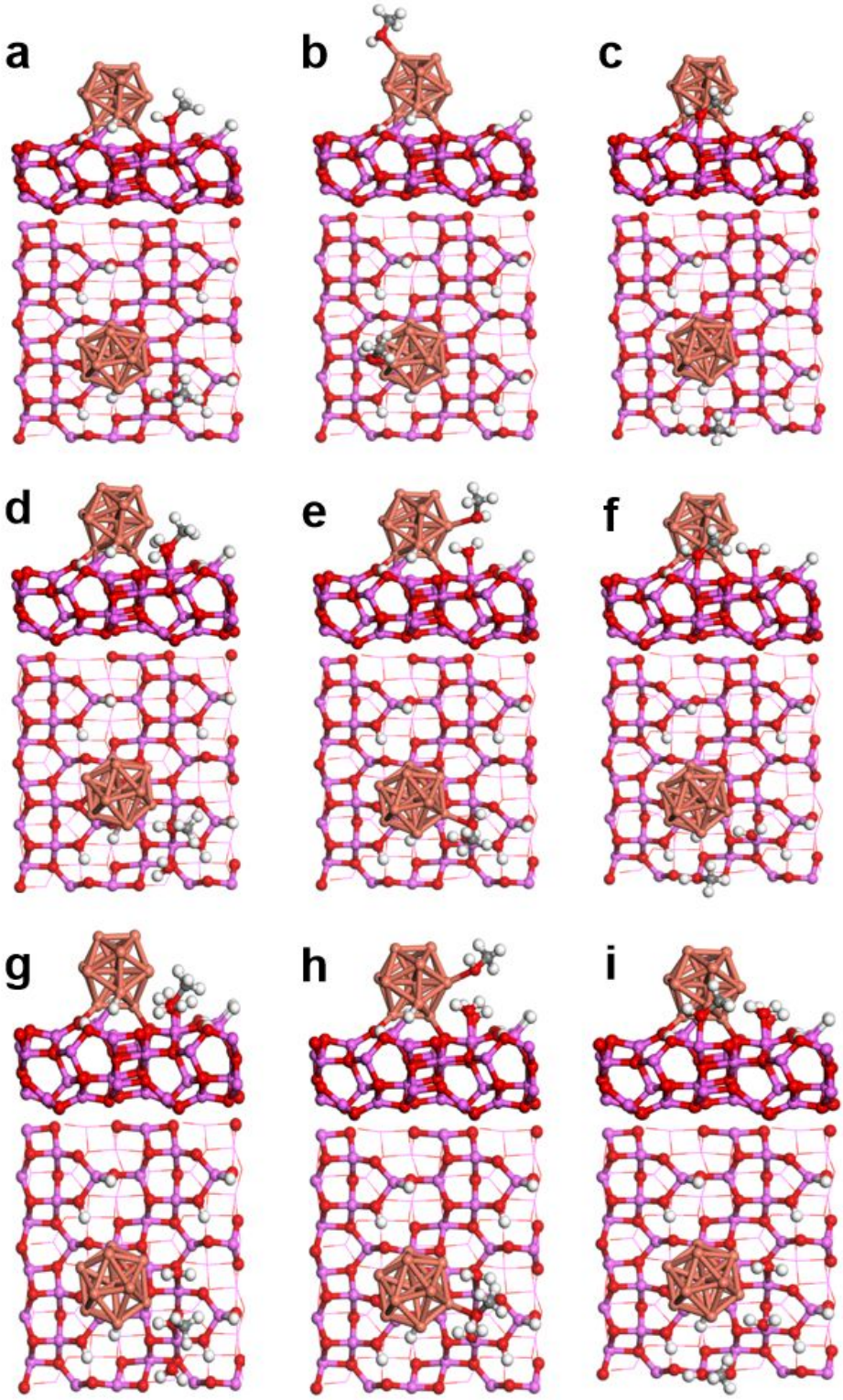

Fig. S17 CH_3OH adsorption configurations in the absence and presence of pre-adsorbed H_2O molecules in side and top view. (a) no H_2O and CH_3OH adsorbed at Cu_{13}/γ-Al_2O_3 interface; (b) no H_2O and CH_3OH adsorbed on Cu_{13}; (c) no H_2O and CH_3OH adsorbed on nearby γ-Al_2O_3 slab; (d) one H_2O pre-adsorbed and CH_3OH adsorbed at Cu_{13}/γ-Al_2O_3 interface; (e) one H_2O pre-adsorbed and CH_3OH

adsorbed on Cu_{13}; (f) one H_2O pre-adsorbed and CH_3OH adsorbed on nearby γ-Al_2O_3 slab; (g) two H_2O pre-adsorbed and CH_3OH adsorbed at Cu_{13}/γ-Al_2O_3 interface; (h) two H_2O pre-adsorbed and CH_3OH adsorbed on Cu_{13}; (i) two H_2O pre-adsorbed and CH_3OH adsorbed on nearby γ-Al_2O_3 slab.

References:

(1) Bansode, A.; Tidona, B.; von Rohr, P. R.; Urakawa, A., Impact of K and Ba promoters on CO_2 hydrogenation over Cu/Al_2O_3 catalysts at high pressure. *Catal. Sci. Technol.* **2013**, 3 (3), 767-778.

(2) Bansode, A.; Urakawa, A., Towards full one-pass conversion of carbon dioxide to methanol and methanol-derived products. *J. Catal.* **2014**, 309, 66-70.

(3) Angelo, L.; Kobl, K.; Tejada, L. M. M.; Zimmermann, Y.; Parkhomenko, K.; Roger, A.-C., Study of CuZnMOx oxides (M = Al, Zr, Ce, CeZr) for the catalytic hydrogenation of CO_2 into methanol. *C. R. Chim.* **2015**, 18 (3), 250-260.

(4) Guo, X.; Mao, D.; Lu, G.; Wang, S.; Wu, G., Glycine-nitrate combustion synthesis of CuO-ZnO-ZrO_2 catalysts for methanol synthesis from CO_2 hydrogenation. *J. Catal.* **2010**, 271 (2), 178-185.

(5) Toyir, J.; de la Piscina, P. R.; Fierro, J. L. G.; Homs, N., Catalytic performance for CO_2 conversion to methanol of gallium-promoted copper-based catalysts: influence of metallic precursors. *Appl. Catal., B* **2001**, 34 (4), 255-266.

(6) Sloczynski, J.; Grabowski, R.; Olszewski, P.; Kozlowska, A.; Stoch, J.; Lachowska, M.; Skrzypek, J., Effect of metal oxide additives on the activity and stability of $Cu/ZnO/ZrO_2$ catalysts in the synthesis of methanol from CO_2 and H_2. *Appl. Catal., A* **2006**, 310, 127-137.

(7) Toyir, J.; de la Piscina, P. R.; Fierro, J. L. G.; Homs, N., Highly effective conversion of CO_2 to methanol over supported and promoted copper-based catalysts: influence of support and promoter. *Appl. Catal., B* **2001**, 29 (3), 207-215.

(8) Xu, J.; Su, X.; Liu, X.; Pan, X.; Pei, G.; Huang, Y.; Wang, X.; Zhang, T.; Geng, H., Methanol synthesis from CO_2 and H_2 over $Pd/ZnO/Al_2O_3$: Catalyst structure dependence of methanol selectivity. *Appl. Catal., A* **2016**, 514, 51-59.

(9) Liang, X.-L.; Dong, X.; Lin, G.-D.; Zhang, H.-B., Carbon nanotube-supported Pd-ZnO catalyst for hydrogenation of CO_2 to methanol. *Appl. Catal., B* **2009**, 88, 315-322.

(10) Hartadi, Y.; Widmann, D.; Behm, R. J., CO_2 Hydrogenation to Methanol on Supported Au Catalysts under Moderate Reaction Conditions: Support and Particle Size Effects. *ChemSusChem* **2015**, 8 (3), 456-465.

(11) Martin, O.; Martin, A. J.; Mondelli, C.; Mitchell, S.; Segawa, T. F.; Hauert, R.; Drouilly, C.; Curulla-Ferre, D.; Perez-Ramirez, J., Indium Oxide as a Superior Catalyst for Methanol Synthesis by CO_2 Hydrogenation. *Angew. Chem., Int. Ed.* **2016**, 55 (21), 6261-6265.

(12) Hu, J.; Yu, L.; Deng, J.; Wang, Y.; Cheng, K.; Ma, C.; Zhang, Q.; Wen, W.; Yu, S.; Pan, Y.; Yang, J.; Ma, H.; Qi, F.; Wang, Y.; Zheng, Y.; Chen, M.; Huang, R.; Zhang, S.; Zhao, Z.; Mao, J.; Meng, X.; Ji, Q.; Hou, G.; Han, X.; Bao, X.; Wang, Y.; Deng, D., Sulfur vacancy-rich MoS_2 as a catalyst for the hydrogenation of CO_2 to methanol. *Nat. Catal.* **2021**, 4 (3), 242.

(13) Song, J.; Liu, S.; Yang, C.; Wang, G.; Tian, H.; Zhao, Z.-j.; Mu, R.; Gong, J., The role of Al doping in Pd/ZnO catalyst for CO_2 hydrogenation to methanol. *Appl. Catal., B* **2020**, 263, 118367.

(14) Yu, J.; Yang, M.; Zhang, J.; Ge, Q.; Zimina, A.; Pruessmann, T.; Zheng, L.; Grunwaldt, J.-D.; Sun, J., Stabilizing Cu+ in Cu/SiO_2 Catalysts with a Shattuckite-Like Structure Boosts CO_2 Hydrogenation into Methanol. *ACS Catal.* **2020**, 10 (24), 14694-14706.

(15) Zhu, J.; Cannizzaro, F.; Liu, L.; Zhang, H.; Kosinov, N.; Filot, I. A. W.; Rabeah, J.; Brueckner, A.; Hensen, E. J. M., Ni-In Synergy in CO_2 Hydrogenation to Methanol. *ACS Catal.* **2021**, 11 (18), 11371-11384.

(16) Jiang, F.; Wang, S.; Liu, B.; Liu, J.; Wang, L.; Xiao, Y.; Xu, Y.; Liu, X., Insights into the Influence of CeO_2 Crystal Facet on CO_2 Hydrogenation to Methanol over Pd/CeO_2 Catalysts. *ACS Catal.* **2020**, 10 (19), 11493-11509.

(17) Yang, T.; Mao, X.; Zhang, Y.; Wu, X.; Wang, L.; Chu, M.; Pao, C.-W.; Yang, S.; Xu, Y.; Huang, X., Coordination tailoring of Cu single sites on C_3N_4 realizes selective CO_2 hydrogenation at low temperature. *Nat. Commun.* **2021**, 12 (1), 6022.

(18) Ruiz Esquius, J.; Bahruji, H.; Taylor, S. H.; Bowker, M.; Hutchings, G. J., CO_2 Hydrogenation to CH_3OH over PdZn Catalysts, with Reduced CH_4 Production. *Chemcatchem* **2020**, 12 (23), 6024-6032.

(19) Liu, T.; Hong, X.; Liu, G., In Situ Generation of the Cu@3D-ZrO_x Framework Catalyst for Selective Methanol

Synthesis from CO_2/H_2. *ACS Catal.* **2019**, 10 (1), 93-102.

(20) Wu, C.; Lin, L.; Liu, J.; Zhang, J.; Zhang, F.; Zhou, T.; Rui, N.; Yao, S.; Deng, Y.; Yang, F.; Xu, W.; Luo, J.; Zhao, Y.; Yan, B.; Wen, X. D.; Rodriguez, J. A.; Ma, D., Inverse ZrO_2/Cu as a highly efficient methanol synthesis catalyst from CO_2 hydrogenation. *Nat. Commun.* **2020**, 11 (1), 5767.

(21) Yang, C.; Pei, C.; Luo, R.; Liu, S.; Wang, Y.; Wang, Z.; Zhao, Z. J.; Gong, J., Strong Electronic Oxide-Support Interaction over In_2O_3/ZrO_2 for Highly Selective CO_2 Hydrogenation to Methanol. *J. Am. Chem. Soc.* **2020**, 142 (46), 19523-19531.

(22) Rui, N.; Zhang, F.; Sun, K.; Liu, Z.; Xu, W.; Stavitski, E.; Senanayake, S. D.; Rodriguez, J. A.; Liu, C.-J. Hydrogenation of CO_2 to Methanol on a $Au^{\delta+}$ -In_2O_{3-x} Catalyst. *ACS Catal.* **2020**, 10 (19), 11307−11317.

(23) Zhang, L.; Liu, X.; Wang, H.; Cao, L.; Huang, C.; Li, S.; Zhang, X.; Guan, Q.; Shao, X.; Lu, J. Size-Dependent Strong Metal−Support Interaction in Pd/ZnO Catalysts for Hydrogenation of CO_2 to Methanol. *Catal. Sci. Technol*. **2021**, 11 (13), 4398−4405.

(24) Cai, Z.; Dai, J.; Li, W.; Tan, K. B.; Huang, Z.; Zhan, G.; Huang, J.; Li, Q. Pd Supported on MIL-68(In)-Derived In_2O_3 Nanotubes as Superior Catalysts to Boost CO_2 Hydrogenation to Methanol. *ACS Catal.* **2020**, 10 (22), 13275−13289.

(25) Sun, K.; Rui, N.; Zhang, Z.; Sun, Z.; Ge, Q.; Liu, C.-J. A highly active Pt/In_2O_3 catalyst for CO_2 hydrogenation to methanol with enhanced stability. *Green Chem.* **2020**, 22 (15), 5059−5066.

(26) Silaghi, M.-C.; Comas-Vives, A.; Coperet, C., CO_2 Activation on Ni/γ-Al_2O_3 Catalysts by First-Principles Calculations: From Ideal Surfaces to Supported Nanoparticles. *ACS Catal.* **2016**, 6 (7), 4501-4505.

(27) Bal, K. M.; Huygh, S.; Bogaerts, A.; Neyts, E. C., Effect of plasma-induced surface charging on catalytic processes: application to CO_2 activation. *Plasma Sources Sci. Technol.* **2018**, 27 (2), 024001.